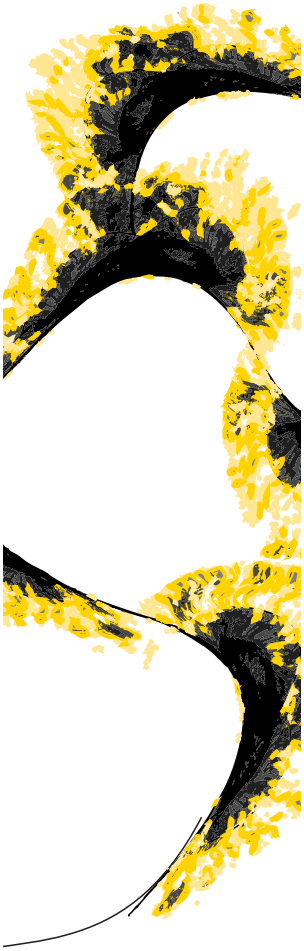

RAM ROBOTICS AND MECHATRONICS

DEVELOPMENT AND EVALUATION OF NOVEL PASSIVE HAPTIC GUIDANCE FOR TELEOPERATED PERCUTANEOUS NEEDLE INSERTION

P. (Patrick) Koehorst

MSC ASSIGNMENT

Committee:
dr. ir. M. Abayazid
M.S. Selim, MSc
dr. V. Kalpathy Venkiteswaran

January, 2025

004RaM2025
Robotics and Mechatronics
EEMCS
University of Twente
P.O. Box 217
7500 AE Enschede
The Netherlands

UNIVERSITY OF TWENTE. | TECHMED CENTRE UNIVERSITY OF TWENTE. | DIGITAL SOCIETY INSTITUTE

Abstract

This study investigates the development and comparison of passive and active haptic guidance techniques for teleoperated needle insertion in percutaneous biopsies. While traditional surgeries leverage kinesthetic and tactile feedback for precision, teleoperated systems often lack these physical connections, resulting in an increased cognitive load for surgeons. Other research has focused on actively guiding the surgeon to desired orientations through the use of virtual springs. These strategies can restrict the amount of control and autonomy of the surgeon. This research proposes a novel passive guidance algorithm using impulse torques, virtual springs and dampers, offering intuitive and dynamic user control without active force application. Comparative experiments were conducted using active guidance methods with varying stiffness levels and the proposed passive guidance algorithm. Performance was evaluated through objective metrics, such as accuracy and execution time, as well as subjective metrics, including user preference and usability. The participants achieved the same success rate of 94% for inserting the needle into small tumors using both algorithms. The used tumor diameters are 10, 8, and 6 millimeters. Metrics describing the accuracy, execution time and the number of used scans did not show a significant difference between the algorithms. The usability of the passive haptic guidance algorithm was significantly worse, albeit still passable. Using the novel passive guidance algorithm, a mean deviation from the center of the tumor of 2.5 millimeters was achieved in 49 seconds. Using the active guidance algorithm, a mean deviation from the center of the tumor of 2 millimeters was achieved in 37 seconds.

Contents

Chapter 1 Introduction

During traditional surgery, surgeons mainly rely on their sense of touch and sight to perform delicate and precise operations [1]. Through their tools, they are in contact with the tissues and can feel the resulting interaction forces. This haptic feedback gives them necessary cues throughout the surgeries, which they rely on for navigation, identification of tissues and anatomical structures, and thus avoiding critical structures. The haptic feedback that they experience is divided into two modalities, kinesthetic and tactile. Kinesthetic feedback is related to the forces exerted on things we touch, while tactile feedback is related to the impact the things we touch have on our skin [2]. For surgeries where the main interaction with the tissues is through surgical tools, kinesthetic is the main type of haptic feedback on which surgeons rely.
During CT-guided surgery, where visual feedback is provided to the surgeon through CT imaging, the patient and surgeon are exposed to harmful radiation [3]. The surgeon's hands are often in proximity to the scanning plane, exposing it to the emitted radiation. Given an annual dose limit of 500 mSv for the hands, Kato et al. calculated that a surgeon may only perform four CT-guided surgeries per year [4]. With the introduction of robot-ed teleoperated surgery, this limit is no longer an issue [5]. The general setup of such a procedure is to have the surgeon operate a leader device that remotely controls a grounded robotic manipulator near the patient. These procedures also allow higher precision and accuracy and do not suffer from tremors compared to manual insertion [6].
However, all physical connections between the surgeon and their tools and therefore also their patients are absent in teleoperated systems. Consequently, the surgeon is unable to feel the tool-tissue interaction forces. This means that surgeons rely solely on their sight to estimate the interaction forces they would normally feel. This can lead to cognitive overload. A way to alleviate this overload is to distribute the information provided to the surgeon across different channels. Efforts have been made to add haptic modalities to the surgical robotic systems [7][8][9]. Both kinesthetic and tactile feedback have been studied and often combined with visual feedback. However, a consensus about the best combination of feedback modalities has not yet been established, as it also depends on the application.
On top of providing transparent feedback to provide a sense of feeling to the surgeon, there is the possibility of assisting the surgeon to navigate to a desired pose during the operation to improve the task performance or reduce the workload. In general robotics, this is referred to as shared control [10]. It can be seen as a compromise between fully autonomous control, which is not desirable in a surgical setting, and manual control, which can be improved. Li et al. introduced three categories of shared control. In Semi-Autonomous Control, the human and autonomous controller control separate state variables. In State-Guidance Shared Control, the state variables are coupled. Instead of controlling the robot directly, the autonomous controller provides guidance in the form of haptic cues to the operator. In State-Fusion Shared Control, the inputs of the human and the autonomous controller are fused by an arbitration mechanism, usually a weighted combination [10]. Of the three categories, State-Guidance Shared Control (SGSC) is the most relevant for robot-assisted surgery, as this form of shared control leaves the final decision for the state variables to the human.
This research will focus on percutaneous biopsies, where a needle is inserted into tissue. It will focus on providing rich and meaningful kinesthetic feedback combined with SGSC.

1.1 Related work

Combining modalities

There are several ways of conveying information to the user that can improve the teleoperated robotic system. These ways are divided into three categories: Vibrotactile, visual, and haptic feedback. These three categories of feedback have been extensively studied in the context of teleoperated surgery. Tholey et al. compared three tissue characterization experiments with a laparoscopic grasper that provides feedback: haptic, visual, or both [11]. They found that the combination of both haptic and visual feedback gave the best results.
Gerovich et al. used a one-degree-of-freedom insertion simulator with a three-layer tissue model, where the objective was to detect the puncture of each tissue layer using haptic cues, visual cues, or both [12]. The haptic cues were simulated using a spring-damper model for every tissue layer and the visual cues showed the layer deflection when piercing through. They also found that the combination of force and visual feedback significantly improved performance.

More recently, Aggravi et al. used an estimation of the depth of the needle acquired through ultrasound imaging to filter out the friction force between the needle and surrounding tissue [8]. With this, they were able to only render the cutting and penetration forces at the tip of the needle as haptic feedback. The user utilized this information to know when it has pierced through a stiff target object. They combined this information with needle direction guidance and compared several combinations of vibrotactile and kinesthetic feedback to convey it to the user. The guidance they used focused on aligning

the tip of the needle with the target using an anisotropic stiffness with low stiffness values along the axis aligned with the needle direction and high stiffness values along other axes. They found the best performance when providing guidance cues through kinesthetic feedback and needle-tip cutting force through cutaneous vibrotactile feedback. They also found that extended periods of cutaneous vibrotactile feedback for guidance becomes unpleasant, degrading the performance. On top of the kinesthetic and vibrotactile feedback, they also visualize the ultrasound image and a real-time reconstruction of the needle pose on a screen.

Transparency and stability

When implementing kinesthetic force feedback, it is desirable to have a system with high transparency. High transparency leads to a high sense of telepresence [13], which equates to the user feeling as though they were actually present and performing the task. However, as transparency through kinesthetic feedback is improved, the risk of instability generally increases [14]. Franken et al. [15] implemented a two-layer controller combining passivity and transparency. This controller guarantees stable behavior of bilateral telemanipulation in the presence of time-varying destabilizing factors. The top layer addresses the desired transparency, while the lower layer ensures passivity by not allowing virtual energy to be generated. This controller expanded upon the Time Domain Passivity Control [16]. An important addition is that it allows for the augmentation of the force feedback to improve performance, which is relevant for guidance.

Virtual fixtures

Guidance methods in teleoperation are often referred to as "virtual fixtures". Virtual fixtures were first introduced by L. Rosenberg [17] and were meant to reduce the mental processing required to perform remote tasks, reduce the workload of sensory modalities, and allow precision and performance to exceed natural human abilities. Virtual fixtures can generally be categorized as either guidance virtual fixtures or forbidden-region virtual fixtures [18]. Guidance virtual fixtures are used to help the user reach or follow a reference. They were used by Betini et al. [19] to assist in a path-following task, and they significantly improved user performance. Huang et al. [20] used a combination of visual feedback and guidance virtual fixtures for a simple teleoperated valve turn task, and also found that virtual fixtures improved the performance. Similar results can be found in other research [8][21][22].

Forbidden-region virtual fixtures (FRVF) are used to prevent the manipulator from entering into forbidden regions of the workspace. They are often implemented as "virtual walls" and typically implemented as spring-damper surfaces [18]. These virtual walls can be implemented either on the leader or the follower side. Abbott [23] investigated the stability of both options and of the combination of the two. They also compared different levels of compliance for the forbidden region, ranging from a relatively low stiffness to completely disallowing movement into the region. The soft virtual wall could be implemented on both the follower and leader side while implementing a hard virtual wall on the follower side led to unstable vibrations of the follower. They also stress the trade-off between submittance (degree of user control) and safety. Li et al. [24] extracted anatomic constraints from real-time 3D images and used FRVF for obstacle avoidance in order to follow a complex path inside a human skull.
Schleer et al. [25] investigated the combination of force reflection and guidance for a general pre-defined trajectory tracking task and found a benefit in avoiding the concealment of information by providing them through different degrees of freedom. Smisek et al. [26] also investigated the same combination, but focused on the effect of inaccuracies of the haptic guidance on the performance. They also stress the difficulty of tuning the haptic guidance so that the operator remains in control but gets guided to a reference position. This difficulty is caused by the fact that the operator has to actively resist or comply with the force pulling it toward the reference, which spans a range of stiffness magnitudes. Another study [27] compared combinations of various levels of haptic transparency and various levels of inaccuracy in the guidance. They found a great increase in task completion time both by offering sufficiently accurate guidance and by increasing haptic transparency. An increase in inaccuracy for the guidance led to a degradation in performance, as it pulled the user in the wrong direction.
In these studies about the combination of force reflection and guidance, the biggest losses in performance arose when using the same DOF for both the force reflection and guidance [25][26][27].

Meli et al. [7] used a 7 DOF Sigma.7 haptic interface capable of outputting torques. They used this torque feedback to maintain the needle at the correct inclination. To achieve this, they use a virtual torsional stiffness multiplied by the difference in orientation between the desired and current needle orientation.

1.2 Contribution and research questions

The main contribution of this paper will be a passive guidance algorithm, as opposed to the active guidance algorithms previously introduced. Instead of using just a torsional stiffness, a decomposition of this system will be utilized. The system is decomposed into three cues, encoding the direction, path, and proximity to the desired orientation. This is realized using a combination of virtual springs and dampers, and allows guiding toward a desired orientation while providing the user with more control. This method allows for more dynamic guidance, as it can guide the user while still enabling ample and intuitive user input. It also addresses the issues noted by [26] and [27], by not actively pulling on the user, but passively guiding them.
Therefore, the research question of this thesis is:

- How can passive haptic guidance in teleoperated needle insertion enhance user control compared to active haptic guidance?

Sub-questions supporting the main question are also defined:

- How can virtual fixtures in the form of impulse directional cues, restrictions of degrees of freedom, and proximity-based damping be used to build a passive guidance system that gives more control to the user to make their own decisions?
- Is there a significant difference in terms of execution time and accuracy between using passive and active guidance?
- Is there a significant difference in user preference regarding ease of use when comparing passive versus active guidance?

For the second and third sub-questions, a null hypothesis is formulated to facilitate statistical testing. H_0: There is no significant difference in the metrics between the passive and active guidance algorithms. We test this against the alternative hypothesis H_1: There is a significant difference in the metrics between the passive and active guidance algorithms.
In Chapter 2, the materials and methods used in this study will be discussed, along with the experimental procedure and evaluation. In Chapter 3, the results of the experiments and the corresponding statistical analyses will be shown. These results will be discussed in Chapter 4, and conclusions will be drawn in Chapter 5.

Chapter 2 Materials and methods

In this chapter the hardware setup used for this research will be introduced. Then, the control strategy will be discussed. After, the passive and active guidance algorithms will be explained. The insertion mode of the algorithm will then be explained followed by the visual feedback provided to the user.
The experimental procedure is then introduced, and with that the metrics and the evaluation of these metrics.
All of the constants used in this study are categorized based on the three algorithms and displayed in Table 1. They will be further elaborated in this chapter.

Table 1: Values and units of all used constants in this study

Algorithm	Parameter	Value	Unit
Active Low	k_{ax}	0	Nm/rad
	k_{ay}	1.0	Nm/rad
	k_{az}	1.0	Nm/rad
	S_{active}	0.225	-
Active High	k_{ax}	0	Nm/rad
	k_{ay}	2.0	Nm/rad
	k_{az}	2.0	Nm/rad
	S_{active}	0.225	-
Passive	D_0	0.8	Nm· s / rad
	B	0.003	rad
	c_{exp}	10.0	-
	k_{caps}	25.0	Nm/rad
	L_{caps}	0.015π	rad
	$L_{caps,exp}$	0.3π	rad
	$\tau_{imp,max}$	0.24	Nm
	t_{imp}	150	ms
	S_{high}	0.3	-
	S_{low}	0.15	-
	S_{dir}	0.1	-
	T_{ramp}	50	ms
	T_D	250	ms
General	α	0.99	-
	D_{max}	5	mm
	d_{tumor}	40	mm
	S_i	0.3	-

2.1 Setup

The setup for this project consists of a leader and follower device. The user manually controls the leader device, which is a 6-DOF Virtuose 6D system developed by HAPTION, situated in Soulge-sur-Ouette, France. It can output a maximum translation force of 21 N and a continuous translation force of 8.5 N. It can also output a maximum rotation torque of 3.1 Nm and a continuous rotation torque of 1.0 Nm. The VIRTUOSE is shown with its world frame Ψ_{Wv} and end-effector frame Ψ_{Ev} in Figure 1.

Figure 1: VIRTUOSE with world frame Ψ_{Wv} and end-effector frame Ψ_{Ev}

The pose of the leader device is used as input for the follower device, which is a 7-DOF Franka Emika robotic arm, developed by Franka Robotics GmbH, situated in Munich, Germany. The Franka with its world frame Ψ_{Wf} and end-effector frame Ψ_{Ef} is shown in Figure 2.
A surgical needle of 152 millimeters in length is mounted on the end-effector of the follower device, with an Ati Nano force/torque sensor mounted at its base. This sensor is developed by ATI Industrial Automation, situated in Apex, USA. It has a sensing range of 70 N and a resolution of $\frac{1}{80}$N in the z-direction, which is the direction along which the force data will be used. The needle is inserted into a PVC phantom representing the liver. A close-up photo of the follower side of the setup can be seen in Figure 3. This is also the starting position of the Franka.

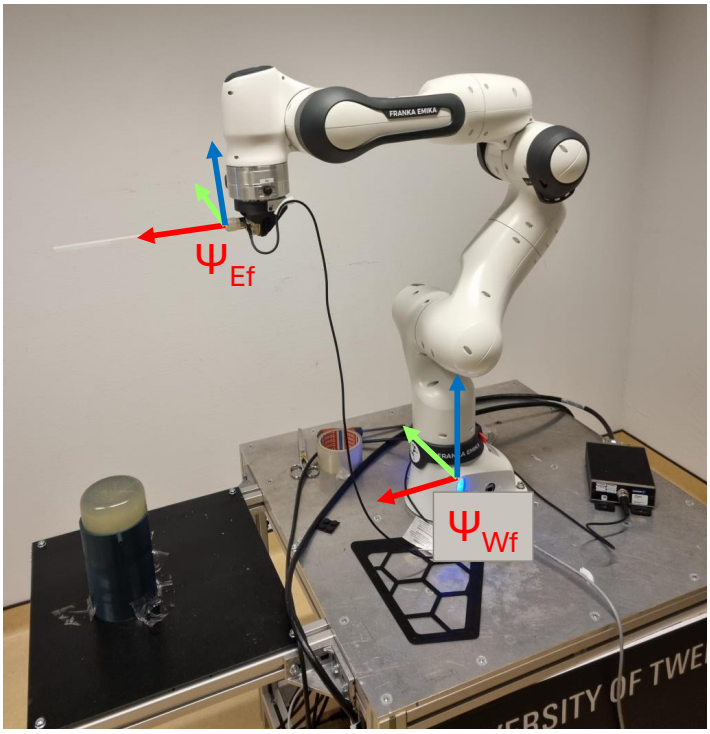

Figure 2: Franka with world frame Ψ_{Wf} and end-effector frame Ψ_{Ef}

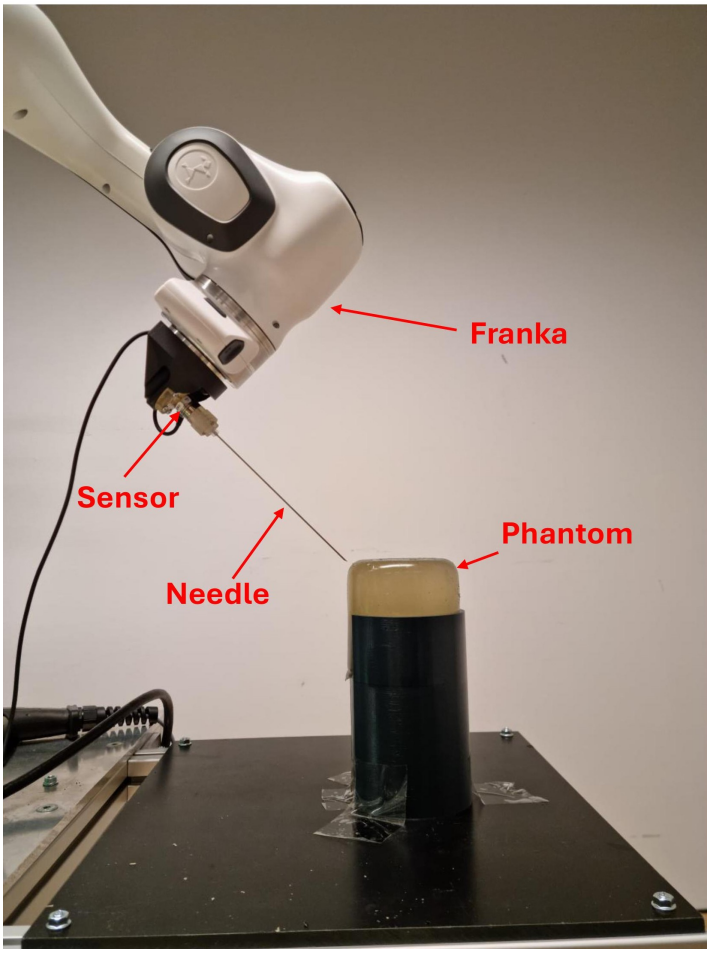

Figure 3: Franka robotic arm with needle attached to force sensor and PVC liver phantom

2.2 Control

A sensitivity factor is used in both alignment and insertion to increase precision. This sensitivity factor effectively scales down the movement of the leader before sending it to the follower. For the insertion, this is straightforward. The axial movement of the end-effector of the leader device is multiplied by sensitivity factor S_i, providing more precision in the insertion depth. For the alignment, it is more complicated. For this, spherical linear interpolation was applied[28]. Spherical linear interpolation is a way of interpolating between two points on a unit circle. The method is illustrated in Figure 4. The figure illustrates the spherical linear interpolation between the points p_0 and p_1. The result of the interpolation is the point p. The trigonometry of this figure is beyond the scope of this study.

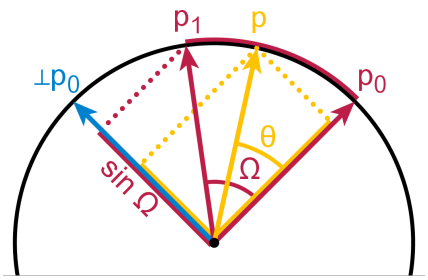

Figure 4: Spherical linear interpolation between points p_0 and p_1.

These points p, p_0, p_1 on the unit sphere are represented by quaternions.
More relevant than the trigonometry, is the equation governing the spherical linear interpolation. Equation 2.1 shows the way the interpolation is calculated for the two points on the unit sphere to get the point p.

$$SLERP(p_0, p_1, t) = p(t) = \frac{sin(1-t)\Omega}{sin(\Omega)} p_0 + \frac{sin(t)\Omega}{sin(\Omega)} p_1 \tag{2.1}$$

.
The interpolation parameter $t, 0 \leq t \leq 1$ thus functions as a weighing parameter for points p_0 and p_1. As t increases, the resulting interpolated point p approaches point p_1 more, which in Figure 4 means an increase in the angle θ.
To use equation 2.1 in the context of this paper, quaternions need to be used instead of points on a unit sphere. This results in equation 2.2 [29].

$$SLERP(q_0, q_1, t) = q(t) = \frac{sin(1-t)\Omega}{sin(\Omega)} q_0 + \frac{sin(t)\Omega}{sin(\Omega)} q_1 \tag{2.2}$$

.
The method used for transforming the pose of the VIRTUOSE is as follows: First, the pose of the VIRTUOSE (Ψ_{Ev}, Figure 1) is transformed to the Franka world frame (Ψ_{Wf}, Figure 2). Then the roll angle of the current pose is set to zero, as the roll is irrelevant to the needle insertion within the assumption of negligible deflection. Then, the quaternion representing the difference between the current and the previous pose is calculated. Spherical linear interpolation is performed between the Identity quaternion and the previously computed difference quaternion, with $t = sensitivity$. The result of this is a scaled difference quaternion that can be post-multiplied with the current pose of the needle (Ψ_{Ef}, Figure 2), which can in turn be transformed into the commanded pose of the Franka.
This commanded pose is given as the equilibrium pose for the built-in *cartesian impedance controller*. The goal of this controller is to alter the system dynamics of the Franka robotic arm, such that, in the presence of external forces and torques at the end-effector $\boldsymbol{F}_{ext}$, the closed loop behaviour is given by

$$\boldsymbol{\Lambda}_d \ddot{\boldsymbol{e}}_x + \boldsymbol{D}_d \dot{\boldsymbol{e}}_x + \boldsymbol{K}_d \boldsymbol{e}_x = \boldsymbol{F}_{ext} \tag{2.3}$$

, with a desired mass $\boldsymbol{\Lambda}_d$, a desired damping $\boldsymbol{D}$, and a desired stiffness $\boldsymbol{K}_d$. These are multiplied by the deviation of the actual Cartesian position from the desired equilibrium point $\boldsymbol{e}_x(t) = \boldsymbol{x}(t) - \boldsymbol{x}_d(t)$. In the example implementation in the libfranka, it is possible to change the values within the desired stiffness matrix $\boldsymbol{K}_d$. A higher stiffness means that the actual pose will more accurately follow the equilibrium pose, at the risk of instability when the deviation $\boldsymbol{e}_x$ reaches a too high value. Tuning this parameter effectively means balancing a trade-off between precision and stability. As this research focuses on inserting a needle into tissue, stability is of great importance. Instability in the system can lead to severe tissue damage. For this reason, some precision is sacrificed in order to ensure stability in this research.

Next, the two control modes of this research will be detailed, being orientation guidance and insertion.

2.3 Active orientation guidance

To compare passive and active guidance, an algorithm for active guidance needs to be implemented. An algorithm similar to the ones developed by Meli et al. [7] and Aggravi et al. [8] will be used, where the guidance is realized using position control. Virtual springs are used between the current orientation and the desired one. As there is a torque that pulls the user toward an orientation, this method is a form of active guidance. The torque is defined in equation 2.4.

$$^{Ev}\boldsymbol{\tau}_{active} = \boldsymbol{K}_{active}\boldsymbol{e}^{d}_{Ef} \tag{2.4}$$

, where $\boldsymbol{K}_{active}$ is defined in equation 2.5.

$$\boldsymbol{K}_{active} = \begin{bmatrix} k_{ax} & 0 & 0 \\ 0 & k_{ay} & 0 \\ 0 & 0 & k_{az} \end{bmatrix} \tag{2.5}$$

The roll component k_{ax} of the stiffness matrix is set to zero, as the roll is fixed. k_{ay} and k_{az} are chosen to be equal. Their values can be found in Table 1. $\boldsymbol{e}$ is obtained from the relative orientation difference between the desired and the current rotation matrices of the franka both expressed in the franka world frame Ψ_{Wf}, as defined in equation 2.6.

$$\boldsymbol{R}^{d}_{Ef} = \boldsymbol{R}^{d}_{Wf} \cdot \boldsymbol{R}^{Wf}_{Ef} \tag{2.6}$$

From this orientation matrix, we can extract the roll, pitch, and yaw and construct the $\boldsymbol{e}^{\boldsymbol{d}}_{\boldsymbol{c}}$ vector:

$$\boldsymbol{e}^{d}_{Ef} = \begin{bmatrix} \psi^{d}_{Ef} \\ \theta^{d}_{Ef} \\ \varphi^{d}_{Ef} \end{bmatrix} \tag{2.7}$$

The active guidance used a sensitivity factor S_{active} for controlling the Franka.

2.4 Passive orientation guidance

The passive guidance algorithm is the novel contribution of this research. It utilizes decoupled virtual springs and dampers to guide the user to the desired needle orientation while also providing more freedom than guidance using only a virtual spring or coupled springs and dampers, as exclusively done in other relevant research. It consists of two control modes: unconstrained and constrained.

2.4.1 Unconstrained

For aligning the needle to a specified desired orientation, damping in two degrees of freedom is applied. These degrees of freedom are the yaw and the pitch expressed in the end-effector frame. When the needle is aligned with the desired orientation, no damping is felt. As the needle rotates away from this orientation, damping gradually increases to signal to the user that it is moving in the wrong direction, while not actively pulling it back to the desired orientation. The torque exerted by this damping is defined in equation 2.8.

$$^{Ev}\boldsymbol{\tau}_{Ev} = D \cdot ^{Ev}\boldsymbol{\omega}_{Ev} \tag{2.8}$$

D is a dynamic damping constant and $\boldsymbol{\omega}$ are the angular velocities around all local axes. The dynamic damping coefficient is graphically shown in Figure 5. It is defined in equation 2.9, with B representing the bounds of the area without damping, D_0 representing a constant value used to create a step function once the bounds are exceeded, and c_{exp} is a constant used to scale up the influence of the orientation error. Their values can be found in Table 1.

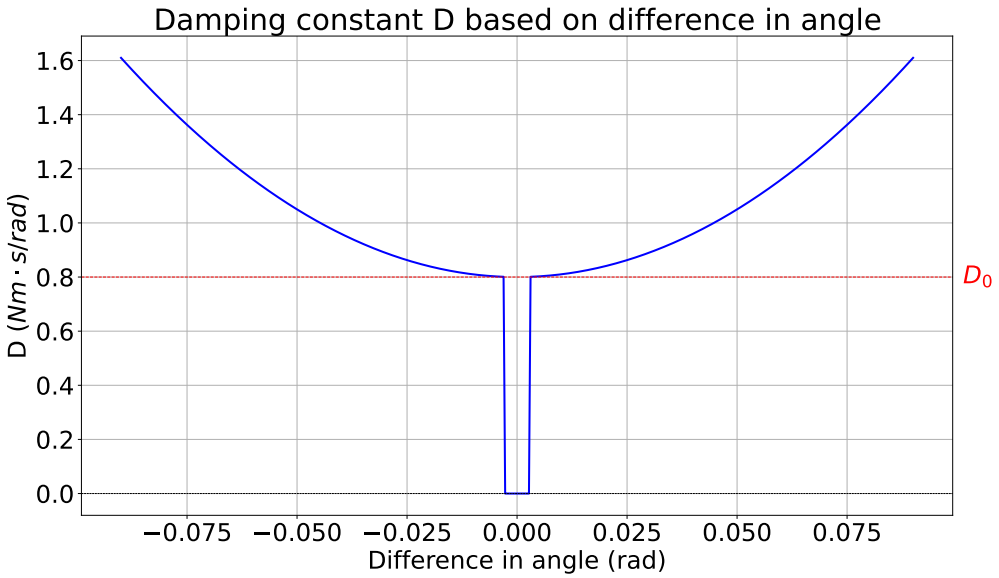

Figure 5: Damping coefficient based on difference in angle

$$D = \begin{cases} 0, & \text{for } |\boldsymbol{e}_{Ef}^{d}| \leq B \\ D_0 + (c_{exp}\boldsymbol{e}_{Ef}^{d})^2, & \text{for } |\boldsymbol{e}_{Ef}^{d}| > B \end{cases} \tag{2.9}$$

When the angle deviation is within the bounds of the no-damping area ($|\boldsymbol{e}_{Ef}^{d}| \leq B$), the sensitivity is set to S_{low}, otherwise it is set to S_{high}. This is done to increase precision when near the tumor.
The roll, pitch, and yaw in $\boldsymbol{e}_c^d$ are defined in the current end-effector frame. Therefore, the torque defined in equation 2.8 is also defined in this frame. As the VIRTUOSE system expects the torque to be expressed in the world frame, one last transformation is needed. This transformation is defined in equation 2.10, where $\boldsymbol{R}_{Ev}^{Wv}$ is the transformation matrix from the end-effector frame of the virtuose to the world frame of the virtuose and ${}^{Wv}\boldsymbol{\tau}_{Ev}$ is the torque acting on the end-effector expressed in the world frame.

$${}^{Wv}\boldsymbol{\tau}_{Ev} = \boldsymbol{R}_{Ev}^{Wv} \cdot {}^{Ev}\boldsymbol{\tau}_{Ev} \tag{2.10}$$

So the unconstrained version of the algorithm allows the user to reach any combination of yaw and pitch in the work-space, while still signaling the desired orientation.
The damping present in the unconstrained mode is sensitive to high-frequency noise. Therefore, an infinite-impulse response (IIR) low-pass filter is used to remove high-frequency noise from the twist of the end-effector. In discrete time, this filter is given by equation 2.11, where T_t is the twist at time t and V_t is the raw twist of the VIRTUOSE. A lower value of α results in a more aggressive filter that rejects more noise, but induces a delay in estimating the true twist. This means that there is a trade-off between noise rejection and fast estimation of the true twist.

$$\boldsymbol{T}_t = \alpha \boldsymbol{V}_t + (1-\alpha)\boldsymbol{T}_{t-1} \tag{2.11}$$

2.4.2 Constrained

If the user deems it necessary, they can press a button on the end-effector which activates a constrained control mode. This control mode effectively decouples the guidance provided in the active guidance method into three separate cues.

Capsule cue

When the buttons is pressed, an axis of rotation is determined. This axis is defined to be perpendicular to the plane formed by the desired needle orientation and the needle orientation at the instant the button is pressed. To calculate the vector representing this axis, the cross-product between the two axes forming the plane is used. This is illustrated in Figure 6. This Figure also shows the frame Ψ_P. The x-axis of this frame is the current needle orientation $\boldsymbol{x}_{cur}$, the y-axis is the cross product between the axis of rotation and $\boldsymbol{x}_{cur}$, and the z-axis is the cross between the x-and y-axis.

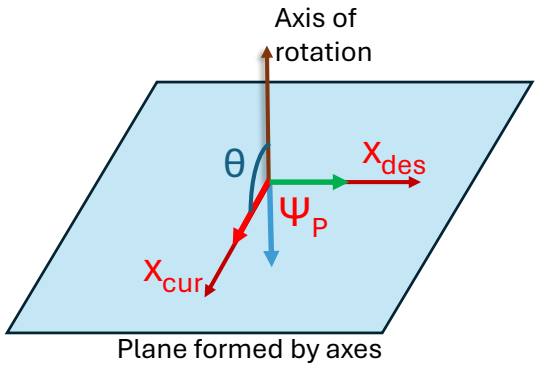

Figure 6: Axis of rotation perpendicular to plane formed by the current x-axis ($\boldsymbol{x}_{cur}$) and the desired x-axis ($\boldsymbol{x}_{des}$). Angle θ between the axis of rotation and $\boldsymbol{x}_{cur}$ and passive frame Ψ_p also displayed.

Rotating around this axis restricts the movement to a curve on which the shortest path to the desired orientation lies. Virtual springs are implemented on either side of the curve to keep the user on the correct trajectory. These springs virtually resemble a capsule around the desired rotational curve, as seen in Figure 7. Since the roll is irrelevant to the system only the pitch and yaw are shown.

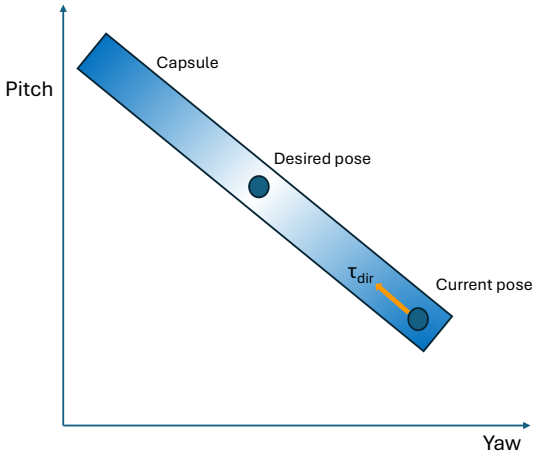

Figure 7: Virtual capsule around desired rotational curve.

To calculate the torque exerted by the capsule, the dot product between the current local x-axis (representing the needle) and the axis of rotation is first calculated. This dot-product represents the cosine of the angle θ between these axes, as both axes are normalized vectors and the dot product is equal to $|a||b|cos(\theta)$. The goal of the constrained mode is to keep the two vectors perpendicular, which effectively results in a rotation of the current x-axis around the axis of rotation (see Figure 6). The torque exerted by the capsule is defined in equation 2.12, , where r is the capsule's radius and k_{caps} is the spring constant of the virtual springs at the borders of the capsule. Their values can be found in Table 1.

$$\tau_{capsule} = \begin{cases} 0, & \text{for } |cos(\theta)| \leq cos(0.5\pi - r) \\ -k_{caps}(cos(\theta) - sign(cos(\theta))cos(0.5\pi - r)), & \text{for } |cos(\theta)| > cos(0.5\pi - r) \end{cases} \tag{2.12}$$

The center of the capsule is defined as $\theta = 0.5\pi$, as this means that the current local x-axis and the rotation axis are perpendicular. The sign of the angle is used to point the spring force in the right direction. This equation makes it so that within the range of the capsule, no torque is applied. Once the borders of the capsule are crossed, a torque is applied to push the user back inside the capsule.
However, when the user makes a sufficient movement through the walls of the capsule, it is possible to break out of this control mode and reactivate the unconstrained mode. In practice, this means that if the angle θ is greater than L_{caps}. The stiffness k_{caps} of the capsule is chosen such that accidentally breaking out of the capsule is very uncommon, but breaking out with a deliberate motion is still easily possible. The radius is chosen such that there is little room to move inside the capsule, constraining the user to the path.

Direction cue

When the button is pressed, the user also receives a brief impulse torque around the axis of rotation in the direction of the desired orientation. The impulse torque first linearly ramps up to a maximum torque of $\tau_{imp,max}$ over a duration of T_{ramp}. It then stays at this maximum torque until $t_{imp} - T_{\text{ramp}}$, where t_{imp} is the total duration of the impulse. After, it linearly ramps back down to zero. This torque profile is described by equation 2.13 and is shown in Figure 8.

$$\tau_{imp}(t) = \begin{cases} \frac{t}{T_{ramp}}\tau_{imp,max}, & \text{if } 0 \leq t \leq T_{\text{ramp}}, \\ \tau_{imp,max}, & \text{if } T_{ramp} \leq t \leq t_{imp} - T_{\text{ramp}}, \\ (1 - \frac{t-(t_{imp}-T_{ramp})}{T_{ramp}})\tau_{imp,max}, & \text{if } t_{imp} - T_{\text{ramp}} \leq t \leq t_{imp}, \\ 0, & \text{otherwise.} \end{cases} \tag{2.13}$$

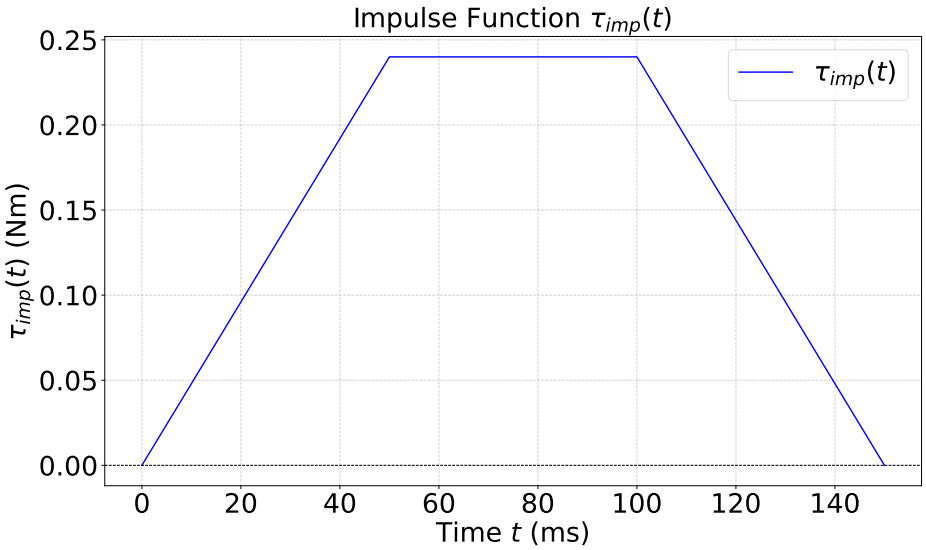

Figure 8: Torque profile of $\tau_{imp}(t)$

The impulse can then be expressed in passive frame Ψ_P, around the x-axis which is the axis of rotation. The impulse is defined in equation 2.14.

$${}^{P}\boldsymbol{\tau}_{dir}(t) = \begin{bmatrix} \tau_{imp}(t) \\ 0 \\ 0 \end{bmatrix} \tag{2.14}$$

The magnitude and duration of the impulse are set at constant, low values. The specific values can be found in Table 1. The reason for having these variables at a low value is that this method is supposed to be passive. The longer and stronger the impulse is, the more the algorithm will converge to the active guidance algorithm. To prevent the impulse from being too similar to the active guidance algorithm, the sensitivity factor is lowered to S_{dir} when the direction is active. The value of this sensitivity can be found in Table 1. This ensures that the movement caused by the impulse on the leader side causes little movement on the follower side. This, in turn, ensures that the user is in control of most of the required orientation adjustments. Keeping the impulse magnitude and duration low and introducing the change of sensitivity results in the change in angle ϕ between the current and desired pose as seen in Figure 9. The angle drops from approximately 0.0833 to 0.0798 radians, which is an angle change of 0.0035 radians. This is deemed sufficiently small to ensure the passive nature of the system, while it is sufficiently big to be perceptible. The direction cue torque τ_{dir} is also visualized in Figure 7 by the orange arrow pointing towards the desired pose.

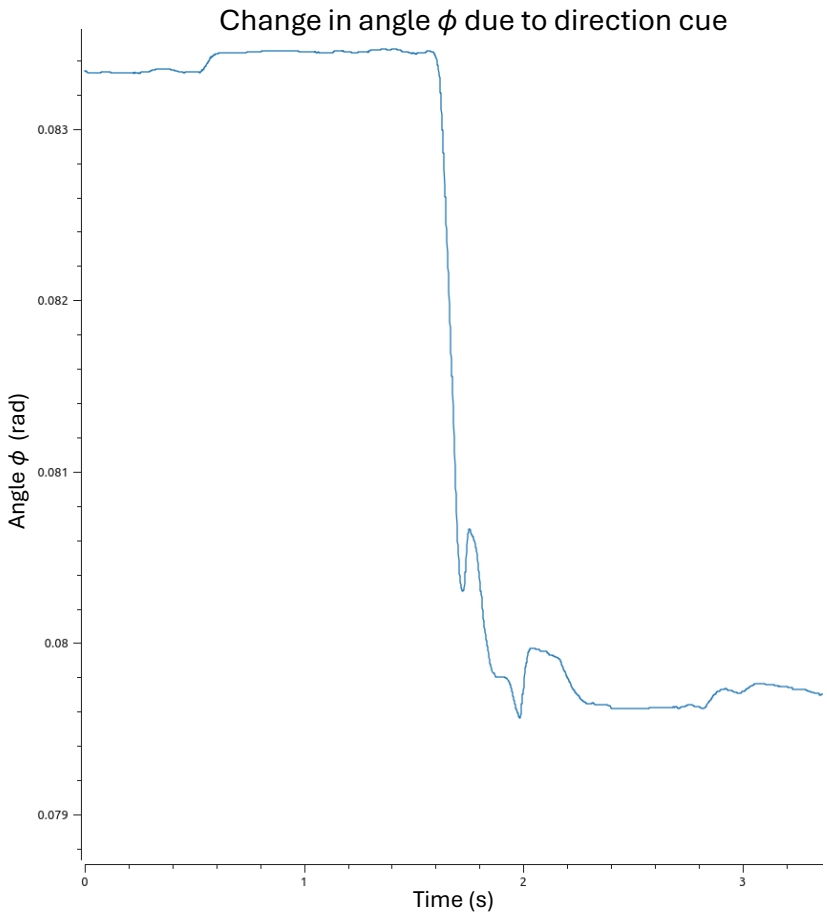

Figure 9: The change in angle between the current and desired pose at the follower side caused by the direction cue. The angle is given on the y-axis in radians against the time in seconds.

Proximity cue

Similarly to the unconstrained mode, gradually ramped damping is applied based on the angular difference from the desired orientation. In this case, the previously defined axis of rotation can be utilized to determine the damping. Since the capsule already constrains movement, damping in only one degree of freedom needs to be applied. This degree of freedom is the rotation around the axis of rotation as defined in 6. The magnitude of the damping can then be related to the angle between the current needle orientation x_{cur} and the desired needle orientation x_{des}. For this, the dot product can be utilized, as shown in equation 2.15. In this equation, ϕ represents the angle between x_{cur} and x_{des}.

$$x_{cur} \cdot x_{des} = |x_{cur}||x_{des}|cos(\phi) \tag{2.15}$$

The torque exerted by the damping is defined in equation 2.17. This torque is defined in the passive frame Ψ_P, and thus also depends on the angular velocity expressed in this same frame. Equation 2.9 can then be modified to only consider this single degree of freedom. This results in equation 2.16. The damping coefficient profile is the same as illustrated in figure 5.

$$D = \begin{cases} 0, & \text{for } |\theta| \leq B \\ D_0 + (c_{exp}\theta)^2, & \text{for } |\theta| > B \end{cases} \tag{2.16}$$

Then, the torque expressed in the passive frame Ψ_P can be defined as in equation 2.17. As in the unconstrained mode, the sensitivity is set to S_{low} when the angle is within the bounds B and set to S_{high} when outside.

$${}^P\tau_{Ev} = D \cdot {}^P\boldsymbol{\omega}_{Ev} \tag{2.17}$$

The proximity cue is also visualized in Figure 7 by the blue color gradient inside of the capsule. This gradient represents the value of D as defined in equation 2.16. The constant c_{exp} is tuned such that the user can move without feeling too much resistance, but can clearly feel the resistance exponentially ramping up as they move away from the desired orientation.

Combining the direction and proximity cues introduced a need to balance perceptibility, stability, and passivity. Initially, the proximity cue was initiated when the direction cue ended. However, this introduced oscillations that could escalate into instability in the system. This is because the end-effector still has a significant angular velocity at this moment caused by the direction cue. A logical solution for this is to initiate the damping at a later moment. However, even with this solution there are still oscillations. This is due to the IIR low-pass filter used to filter the velocity. As defined in equation 2.11, the current twist is calculated using the current measured twist and the previous twist. As seen in Table 1, the value of α is chosen to be 0.99, so a velocity can be propagated for a long time and estimation of the true state is delayed. This means that when the direction cue ends, the residual of previous twists can remain present even in the absence of recent measured twists. Hence, an option is to initiate the damping when the residual of the twist is fully attenuated. In this research, the decision was made to lower the overall damping, the magnitude of the impulse, and the duration of the impulse to reduce the oscillations as much as possible while still having the cues perceptible. Then, the damping is initiated after the period T_D after the cue, such that the velocity is sufficiently attenuated while not forcing the user to wait too long. All of the tuned constants are found in Table 1.

To simplify both control modes, movement in all translational directions is constrained while the needle is being aligned. This is done using stiff virtual springs coupled with dampers, maintaining the end-effector's initial position. Having the two control modes allows the user to choose at any moment how much guidance is necessary to fulfill the task, while never actively pulling the user towards the target.

2.5 Insertion

When the needle is aligned to the desired insertion angle, the user can start moving the end-effector along the axial direction in its local body-fixed frame to start the insertion. While inserting, translational movement along the other dimensions is constrained to minimize forces acting on the tissue surrounding the needle. For the same reason, the rotational movements in all 3 dimensions are constrained as well. Once the user has chosen their insertion orientation, the constraints keep this orientation constant. While inserting, the user feels the axial forces measured by the force sensor located on the needle mount and reflected by the haptic device. This force is processed and transmitted to the user to increase the transparency of the insertion. The force is shown in Figure 10. To create this force profile, the needle was inserted into the tissue and retracted right after.

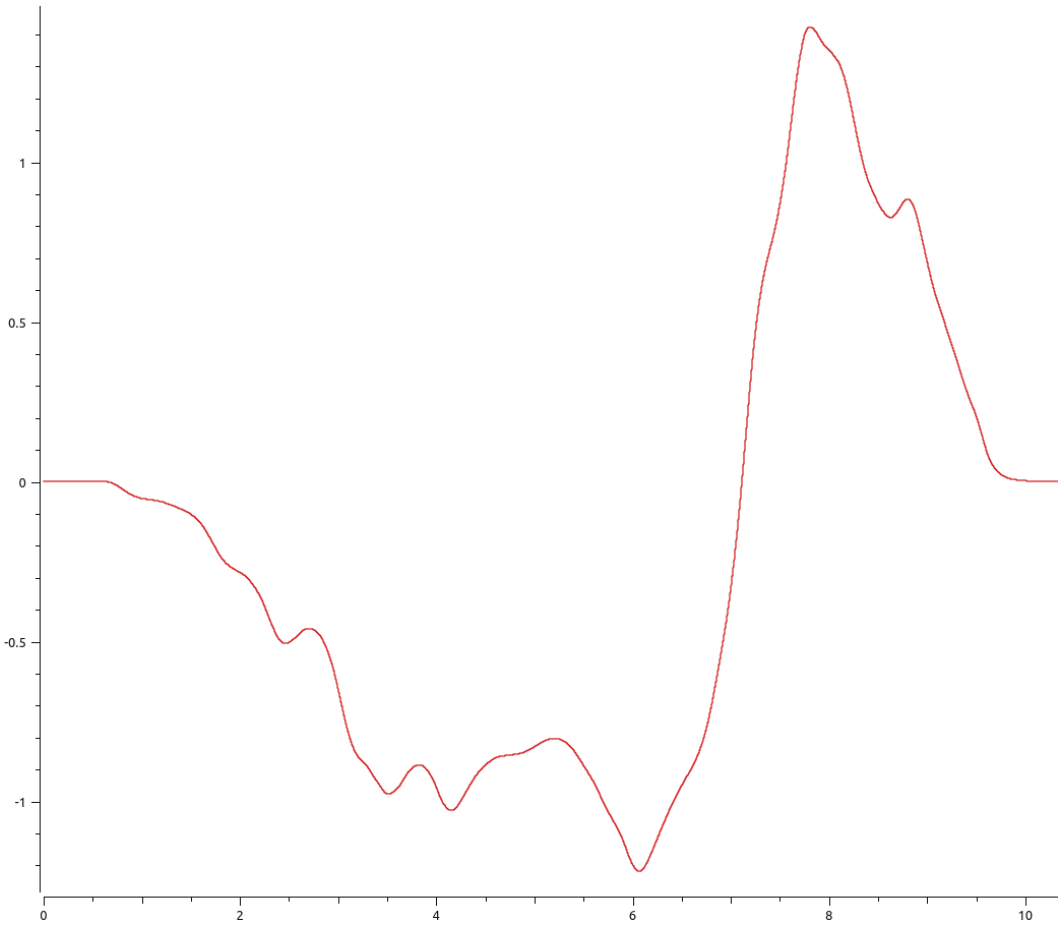

Figure 10: Axial force measured by the sensor in Newtons against time in seconds.

Whenever the user deems it necessary, they can switch back to the constrained mode by pressing the button on the end-effector. This way, they can adjust the direction of the insertion. When the direction is adjusted to their liking, they can resume the insertion by moving the end-effector along the axial direction.
The state diagram of both algorithms is displayed below in Figure 11. As can be seen, the insertion and the conditions to enter and leave this mode are identical for both scenarios. Passive guidance is divided into the previously mentioned unconstrained and constrained modes, while active guidance just has one mode.

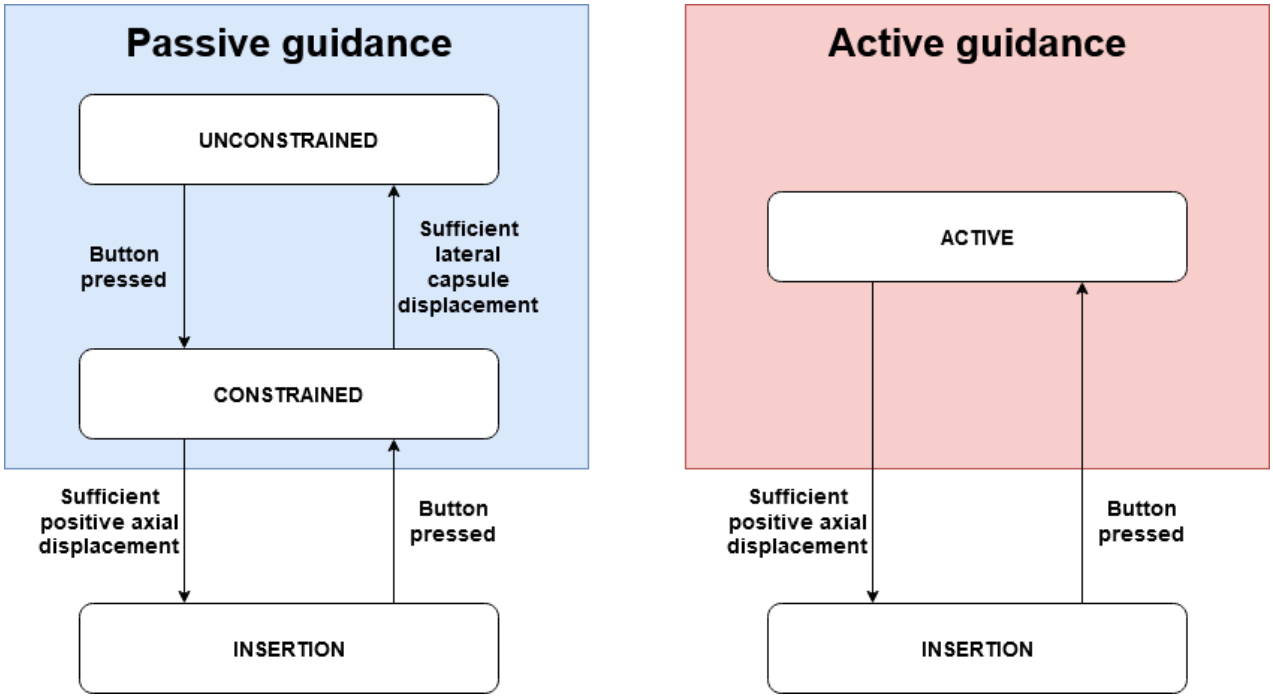

Figure 11: State diagram of both algorithms.

2.6 Visual feedback

Throughout the operation, the user sees the display as seen in Figure 12. On the right, a real-time view from the perspective of the Franka robotic arm can be seen. This view simulates a simplified view from the perspective of the surgeon. Whenever the user requests, a simulated scan of the liver phantom can be made. A top-down- and side-view of the scanned liver are displayed on the left side of Figure 12. In these views, a less opaque version of the liver is displayed, wherein the tumor and needle pose at the instance in time in which the scan is taken can be seen. The scan also provides a drawn between the tip of the needle and the tumor, which assists the user in knowing the misalignment. In the real-time view, the current control mode can be seen in the bottom left. Moreover, the time along with the distance to the tumor along the needle shaft is displayed in the top left.

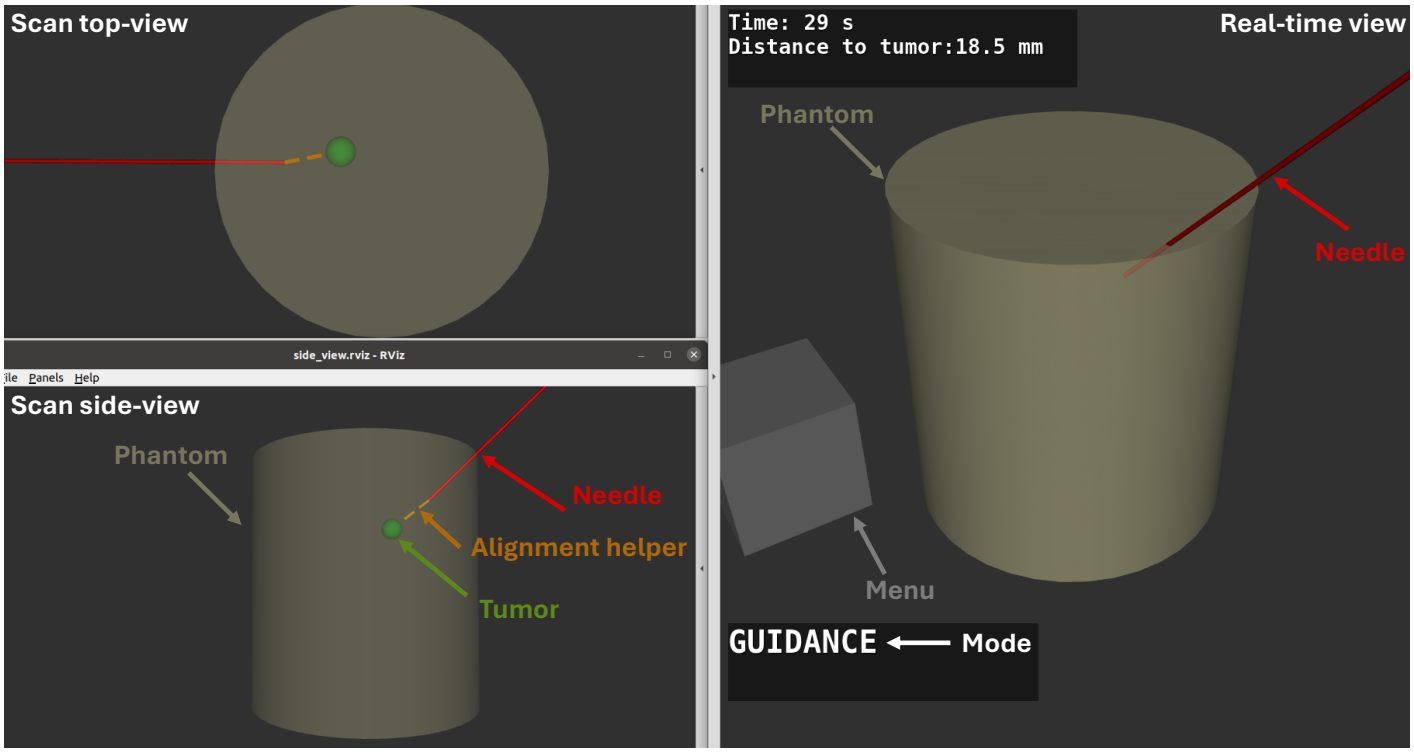

Figure 12: Visual feedback provided to the user. The real-time view of the needle and liver are shown on the right, along with the time, distance to the tumor and current mode. On the left, scans from a top-down and side view are displayed. They show the pose of the needle, tumor, alignment helper, and liver at the instance in which the scan is made.

2.7 Experimental procedure

A total of 7 participants will be recruited for the experiment. None of the participants will have prior experience with the system or the algorithms. The participants will be asked to perform needle insertion tasks using the passive guidance and two versions of the active guidance algorithms for comparison. The option of breaking out of the constrained mode is not provided in this experiment, as they are meant to investigate the constrained mode and its different cues. Therefore, L_{caps} is increased to $L_{caps,exp}$, which is sufficiently high such that it is practically impossible to break out of the constrained mode. To minimize variability due to differences in skill levels, participants will undergo a brief familiarization session with the setup before the experiment begins. They will also receive instructions on how the system and algorithms work, and what their goal is. The task will be performed threefold with the three algorithms, resulting in 9 total trials per participant.
Before the familiarization session, the participants have to pass two tutorials. Both tutorials share the same goal of having to point the needle at 5 pre-defined targets. The layout and order of the targets are shown in Figure 13. These targets are located at four centimeters in front of the starting pose of the needle. The passing condition of the training is to aim the needle at the five targets in ascending order. This has to be done with both the passive and the active algorithms. In the first tutorial they are provided with real-time visual feedback of the needle, tumor, and alignment helper. In the second tutorial their visual feedback is limited to the one shown in Figure 12.

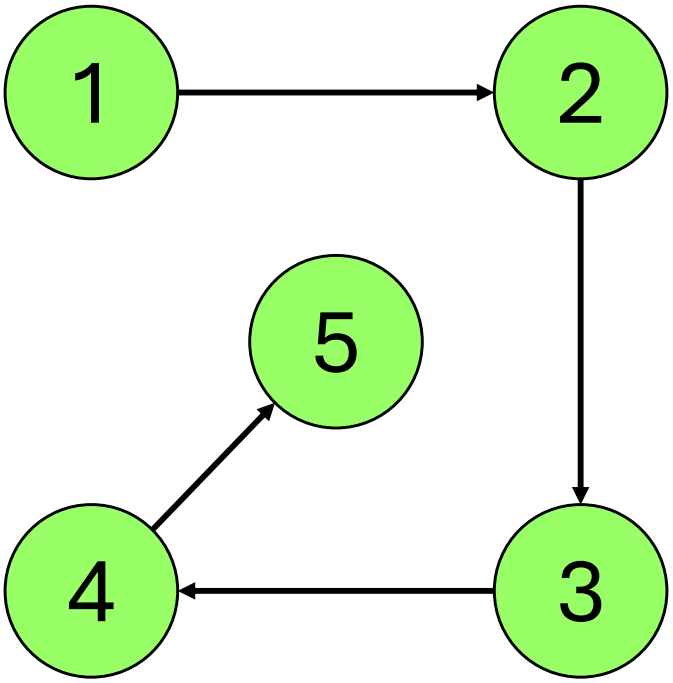

Figure 13: Tutorial targets

The algorithms are integrated into a fully operative setup, where the goal is to reach a simulated target tumor inside the PVC phantom. Initially, the user can start a trial by pressing the button on the end-effector of the VIRTUOSE to activate the guidance mode. For this, there will be three different scenarios:

1. Passive guidance
2. Active guidance algorithm with **low** stiffness values K_a on the diagonal of $\boldsymbol{K}_{active}$
3. Active guidance algorithm with **high** stiffness values K_a on the diagonal of $\boldsymbol{K}_{active}$

The order in which the participants go through these scenarios will be varied, with 3 orders being used:

- 1 - 2 - 3
- 2 - 3 - 1
- 3 - 1 - 2

Once the user decides they are in an adequate orientation, they can enter insertion mode and start inserting. While the user is in insertion mode, there is no difference between both scenarios. The user is constrained to only move in the

direction they had determined before entering insertion mode. The user has the option of switching between the insertion and guidance modes as many times as they desire. They are provided with the visual feedback as shown in Figure 12. The user can request a scan anytime they want, however they are instructed to use them with caution, as they represent CT scans that are harmful if overused. In the scan, they are able to see the pose of the needle, the tumor, and the alignment helper. The task is considered to be fulfilled successfully when the needle punctures the virtual tumor.
To simulate the dynamic environment that is the human body, the virtual tumor shows dynamic movement throughout the task. This will force the user to reorient the needle to realign it with the target, even while already inserted into the phantom. The movement of the tumor is defined to be proportional to the depth of the needle in the phantom. This simulates the displacement of the tumor due to the deformation of the tissue surrounded by the needle. Specifically, the tumor moves based on the relative distance between the needle tip and the tumor along the direction of insertion. This relative distance is calculated using equation 2.18, with d_{tip} and d_{tumor} being respectively the depth of the needle tip and the tumor w.r.t. to the point of insertion, and d_{rel} is this relative distance.

$$d_{rel} = \frac{d_{tip}}{d_{tumor}} \tag{2.18}$$

Using this distance, the location of the tumor changes based on equations

$$\begin{aligned} x &= x_0 + D_{max} d_{rel}^{1.5} \\ y &= y_0 + i_y D_{max} d_{rel}^{1.5} \\ z &= z_0 + i_z D_{max} d_{rel}^{1.5} \end{aligned} \tag{2.19}$$

, where D_{max} represents a maximum displacement of the tumor and i_y and i_z can take values -1 or 1. These variables represent a direction in which the tissue surrounding the needle tip is moved due to tissue deformation. This direction depends on the angle of the bevel tip of the needle. Since this angle is not taking into account here, three different combinations of the variables i_y and i_z are chosen for the three different trials. The exponent of 1.5 is chosen to simulate the increased movement of the tumor when the needle approaches it, due to more tissue displacement closer to the needle tip. Experimental data has shown displacements ranging from 0.2 to 3 millimeters for an insertion depth of 15 millimeters [30]. The average displacement was around 1 to 1.5 millimeters. For the insertion depth of 40 millimeters used in this research, a maximum displacement is chosen accordingly at 5 millimeters. The second variable that changes between the trials is the tumor size. Liver tumors can have a diameter anywhere between 0.1 and 20 centimeters [31]. For this study, tumor sizes are chosen to be at the bottom end of this range. They are displayed in Table 2. Lastly, the initial tumor location is varied between each trial.

Table 2: Tumor size per trial

Trial	**Tumor diameter (mm)**
1	10
2	8
3	6

2.7.1 Metrics

The evaluation of the performance of both algorithms will be done using both objective and subjective metrics.

- Objective metrics
  - Accuracy: Measured by the Euclidean distance between the center of the target tumor and the tip of the needle after the user is completely done with the insertion. This total error is calculated as $e_{tot} = ||\boldsymbol{p_{tip}} - \boldsymbol{p_{tumor}}||$
  - Alignment accuracy: Measured as the Euclidian distance between the center of the target tumor and the tip of the needle, but with the axial distance not included. So this is the lateral error and is calculated as $e_{lat} = || \begin{pmatrix} p_{tip,y} \\ p_{tip,z} \end{pmatrix} - \begin{pmatrix} p_{tumor,y} \\ p_{tumor,z} \end{pmatrix} ||$
  - Success: Boolean depicting whether or not the tip of the needle is inside of the tumor when the trial is finished. When e_{tot} is smaller than the tumor radius, its value is 1. Otherwise, the value is 0.
  - Number of scans: The number of scans made during the trial
  - Execution time: The time taken by the participant to reach the target tumor, to a maximum of 100 seconds. The time is measured from the first button press.
- Subjective metrics
  - Usability: How simple and intuitive is the system to effectively complete the task with minimal effort and confusion? The usability is measured using the System Usability Scale [32].

2.7.2 Evaluation

In order to compare the performance of the three guidance algorithms across all of these metrics, a repeated measures anova test is conducted. The repeated measures anova test is appropriate as each participant will perform tasks using all three algorithms, allowing us to account for within-subject variability [33]. This statistical test will determine if there are significant differences in the performance metrics between the algorithms. As previously stated, the null hypothesis and alternative hypothesis are defined as

- H_0: There is no significant difference among the means of the metric between the passive and active guidance algorithms
- H_1: There is a significant difference among the means of the metric between the passive and active guidance algorithms

In statistical testing, it is common to use a significance level $\alpha = 0.05$. However, since the population size in this research is very limited, a looser significance level $\alpha = 0.10$ is used. This generally reduces the chance of type 2 errors, where true differences are not detected [34]. However, it comes at the cost of increasing the chance of type 1 errors, where differences are detected that do not exist. In a small dataset like the one used in this research, higher significance thresholds tend to balance these errors well [35]. The null hypothesis is rejected if the p-value obtained from the anova test is greater than α.

For the subjective evaluation of each guidance algorithm, participants will complete post-task questionnaires using a Likert scale [36]. Each subjective measure is rated on a 5-point Likert scale, ranging from 1 = "Strongly Disagree" to 5 = "Strongly agree". The questions used in the questionnaire will be based on the System Usability Scale [32], which is a standardized scale to assess usability. The questions can be seen in Table 6.

Table 3: System Usability Scale (SUS) Questions

Q	Question	Strongly Disagree	Strongly Agree
1	I think that I would like to use this method frequently	1	5
2	I found this method unnecessarily complex	1	5
3	I thought this method was easy to use	1	5
4	I think that I would need the support of a technical person to be able to use this method	1	5
5	I found this method very intuitive	1	5
6	I thought there was too much inconsistency in this method	1	5
7	I would imagine that most people would learn to use this method very quickly	1	5
8	I found this method very awkward to use	1	5
9	I felt very confident using this method	1	5
10	I needed to learn a lot of things before I could get going with this method	1	5

The odd questions have a negative tone and the even questions have a positive tone. For the odd questions, 1 is subtracted from the raw score, and for the even questions, the raw score is subtracted from 5. This results in all question scores being in the range $(0, 4)$, with a higher score being more positive. The final standard SUS score can then be calculated using equation 2.20.

$$SUS = 2.5(sum(Q1, Q2, \cdots, Q9, Q10)) \tag{2.20}$$

This results in in the standard SUS score being in the range of $(0, 100)$. A review of 446 surveys and usability study found a mean SUS score of 68 with a standard deviation of 12.5 [37]. They consider this to be the passing score for the System Usability Scale.

By averaging the scores across participants for each algorithm, the subjective measures can again be compared the repeated measures ANOVA test to determine whether there are statistically significant differences in user experience between the three algorithms. For this, the same null and alternative hypothesis are considered.

Chapter 3 Results

3.1 Introduction

This chapter presents the results of the experiment designed to compare the performance of passive and active guidance algorithms needle insertion. The results are divided into objective and subjective metrics, followed by statistical analyses to assess differences between experimental conditions. The findings are summarized and visually displayed in this chapter. One participant was unable to complete the trials using the passive guidance algorithm due to a lack of understanding, making it impossible to make a comparison. Therefore, they are treated as an outlier and not taken into account in the results.

3.2 Objective Metrics

The objective metrics evaluated in this experiment are

- Success
- Accuracy; This metric is measured using the total error in millimeters
- Alignment accuracy; This metric is measured using the alignment error in millimeters
- Number of scans
- Execution time

Table 4 provides the mean and standard deviation for the three algorithms: active guidance with high stiffness, (Active High) active guidance with low stiffness (Active Low), and passive guidance (Passive). Box plots of these results are shown in figure 14. The passive guidance algorithm shows one significant outlier in all metrics except the success rate. The active guidance algorithm with high stiffness also contains a smaller yet still significant outlier for the total and alignment error.

Table 4: Means and standard deviations of the objective metrics

Algorithm	Success	Total Error (mm)	Alignment Error (mm)	Number of scans	Time (s)
Active Low	0.94 ± 0.14	2.01 ± 0.34	1.92 ± 0.32	2.11 ± 1.05	39.31 ± 3.85
Active High	0.94 ± 0.14	2.0 ± 0.5	1.89 ± 0.54	1.83 ± 0.72	37.2 ± 9.52
Passive	0.94 ± 0.14	2.51 ± 1.41	2.25 ± 1.18	2.72 ± 2.33	48.99 ± 18.18

To analyze differences in the metrics across the three conditions, a repeated measures ANOVA test was performed. The results of this can be seen in table 5.

Table 5: Results of repeated measures anova test for all variables. Degrees of freedom, testing statistic F and the p-value are displayed

Variable	df	F	p
Success	2	0	1.0
Accuracy	2	0.56	0.59
Alignment accuracy	2	0.34	0.72
Number of scans	2	1.14	0.36
Execution Time	2	1.24	0.33

None of the metrics show a significant p-value ($p < 0.10$). This means that the null hypothesis is rejected. Thus, the means of the metrics do not significantly differ between the algorithms.

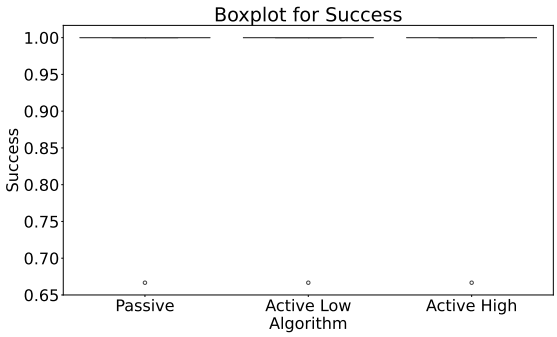

(a) Box plot for success metric

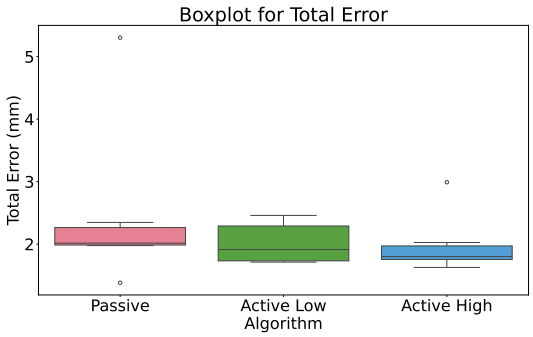

(b) Box plot for total error metric

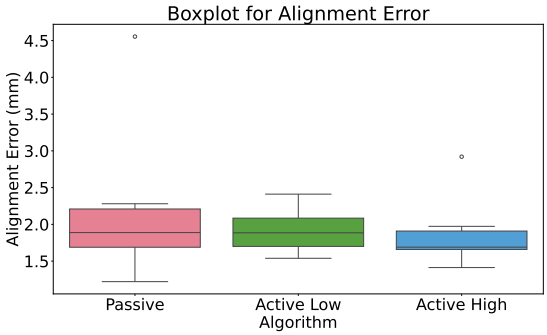

(c) Box plot for alignment error metric

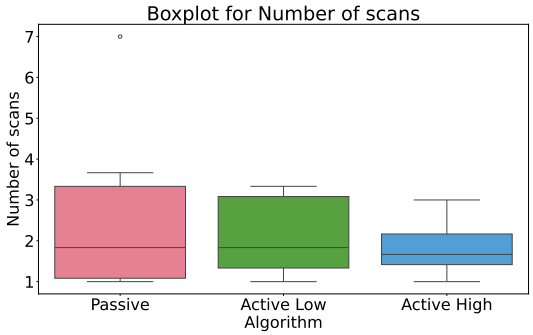

(d) Box plot for number of scans metric

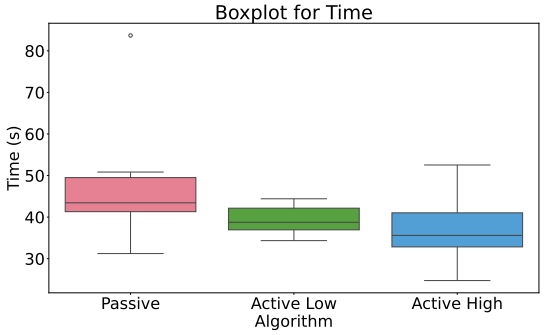

(e) Box plot for time metric

Figure 14: Box plots of the five measured metrics for the three algorithms

3.3 Subjective Metrics

The subjective metrics are measured using the System Usability Scale measured on a Likert scale. The resulting SUS scores with their standard deviations are displayed in table 6

Algorithm	SUS score
Passive	63.33 ± 24.83
Active Low	90.83 ± 5.85
Active High	82.50 ± 12.14

Table 6: SUS scores with their standard deviations for the three algorithms

In figure 15, a visual comparison in the form of box plotsof the SUS scores of the three algorithms are displayed.

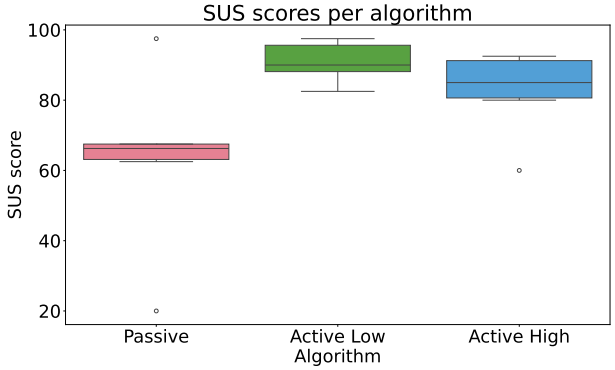

Figure 15: Box plot of the SUS scores for the three algorithms

As stated before, an average of 68 with a standard deviation of 12.5 was found for the SUS scores across 446 studies. Using this as a benchmark, both the active guidance algorithm with low and high stiffness show good usability, with the low stiffness variant excelling above. The mean SUS score of the passive guidance algorithm falls just short of the benchmark, but is within the standard deviation. Notably, there are two outliers present in the SUS scores of this algorithm. The high outlier is a score of 97.5 and the low outlier is a score of 20. Another outlier is seen in the active guidance algorithm with high stiffness, being a score of 60.
Again, statistical analysis was performed on these results. A repeated measures ANOVA test is used to compare the means of the SUS scores between the algorithms. The result of this can be found in table 7.

Table 7: Results of repeated measures anova test for the SUS score. Degrees of freedom, testing statistic F and the p-value are displayed

Variable	df	F	p
SUS score	2	3.68	0.063

A p-value of 0.063 is found for the repeated measures ANOVA test. With the chosen significance threshold of $\alpha = 0.10$, this means that the null hypothesis is rejected. Thus, there is a significant difference between the means of the SUS score between the algorithms. To find out where this difference lies, a post-hoc analysis using pairwise comparisons with the same significance threshold of $\alpha = 0.10$ was conducted to evaluate the differences between the three algorithms. The results of this are displayed in table 8. A significant p value below the significance threshold is found for the difference between the active guidance algorithm with low stiffness and the passive guidance algorithm. This signifies that the means of these algorithms differ significantly.

Table 8: Results of post-hoc pairwise analysis of SUS scores. Hedges' g and p-value are displayed

Algorithm A	Algorithm B	hedges' g	p
Active High	Active Low	-0.81	0.14
Active High	Passive	0.91	0.20
Active Low	Passive	1.41	0.064

To further investigate the developed passive guidance algorithm, two questions from the SUS are slightly altered and asked once more for the three separate cues. The questions are displayed in table 9.

Table 9: Specific questions about the cues

Q	**Question**	**Strongly Disagree**	**Strongly Agree**
1	I found the cue very intuitive	1	5
2	I did not feel confident using the cue	1	5

As for the SUS, 1 is subtracted from the score of the positive question Q1 and the score of negative question Q2 is subtracted from 5. The final score is then calculated using

$$score = 1.25(Q1 + Q2) \tag{3.1}$$

, resulting in a score between 0 and 10, with 10 being the best possible score. These scores are displayed in table 10. They are also visually displayed in figure 16.

Cue	SUS score
Direction	7.50 ± 1.37
Capsule	6.875 ± 1.90
Proximity	8.125 ± 2.34

Table 10: Subjective scores with their standard deviations for the three cues of passive guidance

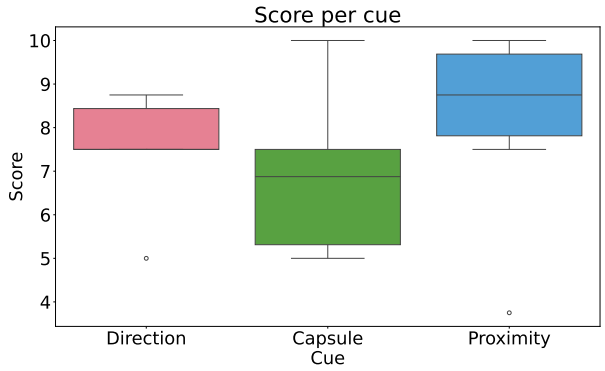

Figure 16: Box plot of the subjective scores for the three cues

There appears to be no big difference in terms of usability between the three cues. All three cues are given a sufficient score. The mean score of the proximity cue is the highest, while the mean score of the capsule cue is the lowest. Both the direction and proximity cue have a big negative outlier. These results are only meant to give further insight into the usability of the separate cues and will therefore not be statistically analyzed.
Finally, the participants filled in a general questionnaire, in which they also stated their preferred algorithm. The result of this can be seen in figure 17. Of the six participants, three voted for the active guidance algorithm with low stiffness, one voted for the active guidance with high stiffness, one for the passive guidance, and one for active guidance without a preference for stiffness.

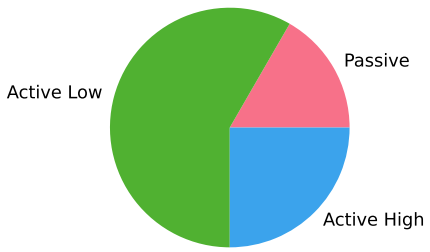

Figure 17: Pie chart of user preference of algorithm

Chapter 4 Discussion

This research has shown the potential of using the VIRTUOSE to control a Franka robotic arm in a percutaneous needle insertion task. With both the state-of-the-art active guidance algorithm and the novel passive guidance algorithm, sufficient accuracy for tumor targeting within half of the time limit set at 100 seconds. Although no significant differences were found for any of the objective metrics between the three algorithms, their mean and median values show some small differences. For all metrics, the passive guidance shows slightly worse mean values than the other two algorithms. The reason why this difference does not show up in the anova test might be due to the limited size of the dataset or the difference not being sufficiently big. The design of the passive guidance algorithm should facilitate a higher degree of user control compared to active guidance. This study analyses the effects on the usability, precision, and efficiency when using this algorithm. While the mean precision and efficiency show a slight decrease, the success rate of reaching the tumor with the needle tip does not suffer. As the tumor sizes in this study were chosen to reflect the bottom end of the range of tumor sizes found in clinical scenarios, this shows good potential for clinical use. Tumor sizes as small as 6 millimeters in diameter were successfully penetrated by the needle. The mean usability of the passive guidance algorithm is worse than for the other algorithms. There is a significant difference in usability between the passive guidance algorithm and active guidance algorithm, where the latter outperforms the former. A large between-subject variance can be seen for the passive guidance algorithm, with one participant giving an almost perfect score and another giving an extremely poor score. Not surprisingly, the participant that felt the system to have poor usability was also the one responsible for the significant negative outliers in most metrics. Generally, the participants took longer to get the grasp of the passive guidance algorithm during the training phases. Initial difficulties always included ensuring that the end-effector was not gripped too tightly. If it is, it is difficult to perceive the cues, especially the direction cue. All of the participants were able to pass the two training phases and felt ready to perform the experiments after.
The number of scans metrics was introduced to indicate a level of confidence about the alignment based purely on the haptic feedback. If the participant is not confident in the feedback, they would presumably ask for more scans to confirm. The participants were instructed to keep their use of scans to a minimum if possible, as they represent harmful CT-scans. Overall, the number of scans for each algorithm was low. The average number of scans is higher for the passive guidance compared to the active algorithms, suggesting a lack of confidence. Given the lower usability score and the lower mean errors for the passive guidance algorithm, these metrics align well.

4.1 Limitations

A big limitation of this study is the limited population size. Having a small population size limits the validity of the results and subsequent statistical analysis. With such a limited dataset, the risk of type 2 errors is increased, as there is a lack of statistical power. The biggest reason for this limitation was a lack of time. Another limitation of the study is the lack of needle pose tracking. For the tip pose, an infinitely stiff needle is assumed. In practice, the needle will bend due to the reaction forces from the tissue. Therefore, there is always a deviation between the actual tip pose and the simulated tip pose.
A limitation of the algorithms used in this study is the use of Euler angles as the basis of the active guidance. Euler angles have the inherent risk of singularities, also known as gimbal lock [38]. These singularities can occur as angles approach 90 degrees, depending on the order in which the Euler parametrization is represented. In the case of needle insertion as used in this study, these singularities could mostly be avoided by limiting the angles of both the leader and follower end-effectors. However, in some cases when the required angle change to reach a tumor is sufficiently large, this limitation becomes quite prominent. Since there is no clutching used in this study, this leads to a limited workspace of the VIRTUOSE end-effector. A final limitation of the study is the use of the cartesian impedance controller. The inherent balancing between the accuracy and stability makes it difficult to improve the performance of the algorithms. In this study, the stiffness of the controller was raised up to the highest value such that stability was ensured but the accuracy was maximized.

Chapter 5 Conclusion

5.1 Conclusion

A passive guidance algorithm was developed that gives the user more control compared to an active guidance algorithm. Some usability was sacrificed to achieve the added user control. The participants achieved the same success rate for needle insertion in small tumors using both algorithms. Metrics describing the accuracy, execution time and the number of used scans did not show a significant difference between the algorithms. Using the novel passive guidance algorithm, a success rate of 94% was reached with a mean deviation from the center of the tumor of 2.5 millimeters in 49 seconds.

5.2 Recommendations and Future work

In the future, a larger population size should be used to have a better validation of the system. Initially, 12 participants were meant to participate in this research, so this would be a good place to start. Good care needs to be taken in training the participants and making sure they grasp the passive guidance algorithm to minimize outliers. For accurate targeting of the tumor, tracking or estimation of the needle pose and tumor would be necessary, because the desired orientation depends on these poses. Using a model the bending of the needle and the movement of the tumor due to tissue deformation could facilitate this. For this, the bevel tip and its orientation also need to be taken into account.
In future work, using other orientation representations without the risk of singularities should be considered, like rotation matrices or quaternions. This can expand the workspace of the leader device and improve overall consistency in feedback. In the constrained mode of the passive guidance algorithm the dependency on Euler angles has already been removed by using the axis of rotation. Something similar could be implemented for the active guidance algorithm and the unconstrained mode. Finally, using or developing a controller that allows for higher accuracy without risk of instability, or adding a passivity layer ensuring stability could alleviate the limitations in accuracy.

Chapter 6 Bibliography

[1] Mohsin I. Tiwana, Stephen J. Redmond, and Nigel H. Lovell. "A review of tactile sensing technologies with applications in biomedical engineering". In: *Sensors and Actuators A: Physical* 179 (June 1, 2012), pp. 17–31. ISSN: 0924-4247. DOI: 10.1016/j.sna.2012.02.051. URL: https://www.sciencedirect.com/science/article/pii/S0924424712001641 (visited on 06/05/2024).

[2] Issam El Rassi and Jean-Michel El Rassi. "A review of haptic feedback in tele-operated robotic surgery". In: *Journal of Medical Engineering & Technology* 44.5 (July 3, 2020). Publisher: Taylor & Francis _eprint: https://doi.org/10.1080/03091902 pp. 247–254. ISSN: 0309-1902. DOI: 10.1080/03091902.2020.1772391. URL: https://doi.org/10.1080/03091902.2020.1772391 (visited on 04/08/2024).

[3] Chun-Feng Cao et al. "CT Scans and Cancer Risks: A Systematic Review and Dose-response Meta-analysis". In: *BMC Cancer* 22 (Nov. 30, 2022), p. 1238. ISSN: 1471-2407. DOI: 10.1186/s12885-022-10310-2. URL: https://www.ncbi.nlm.nih.gov/pmc/articles/PMC9710150/ (visited on 06/12/2024).

[4] R. Kato et al. "Radiation dosimetry at CT fluoroscopy: physician's hand dose and development of needle holders". In: *Radiology* 201.2 (Nov. 1996), pp. 576–578. ISSN: 0033-8419. DOI: 10.1148/radiology.201.2.8888264.

[5] Stephen B. Solomon et al. "Robotically Driven Interventions: A Method of Using CT Fluoroscopy without Radiation Exposure to the Physician". In: *Radiology* 225.1 (Oct. 2002), pp. 277–282. ISSN: 0033-8419. URL: https://www.ncbi.nlm.nih.gov/pmc/articles/PMC3107539/ (visited on 06/05/2024).

[6] Ilse M. Spenkelink et al. "Evaluation of the performance of robot assisted CT-guided percutaneous needle insertion: Comparison with freehand insertion in a phantom". In: *European Journal of Radiology* 162 (May 1, 2023), p. 110753. ISSN: 0720-048X. DOI: 10.1016/j.ejrad.2023.110753. URL: https://www.sciencedirect.com/science/article/pii/S0720048X23000670 (visited on 06/05/2024).

[7] Leonardo Meli, Claudio Pacchierotti, and Domenico Prattichizzo. "Experimental evaluation of magnified haptic feedback for robot-assisted needle insertion and palpation". In: *The International Journal of Medical Robotics and Computer Assisted Surgery* 13.4 (2017). _eprint: https://onlinelibrary.wiley.com/doi/pdf/10.1002/rcs.1809, e1809. ISSN: 1478-596X. DOI: 10.1002/rcs.1809. URL: https://onlinelibrary.wiley.com/doi/abs/10.1002/rcs.1809 (visited on 04/23/2024).

[8] Marco Aggravi et al. "Haptic teleoperation of flexible needles combining 3D ultrasound guidance and needle tip force feedback". In: *IEEE Robotics and Automation Letters* 6.3 (2021), p. 4859. DOI: 10.1109/LRA.2021.3068635. URL: https://inria.hal.science/hal-03164691 (visited on 04/23/2024).

[9] Allison M. Okamura. "Haptic Feedback in Robot-Assisted Minimally Invasive Surgery". In: *Current opinion in urology* 19.1 (Jan. 2009), pp. 102–107. ISSN: 0963-0643. DOI: 10.1097/MOU.0b013e32831a478c. URL: https://www.ncbi.nlm.nih.gov/pmc/articles/PMC2701448/ (visited on 06/05/2024).

[10] Gaofeng Li et al. "The Classification and New Trends of Shared Control Strategies in Telerobotic Systems: A Survey". In: *IEEE Transactions on Haptics* 16.2 (Apr. 2023). Conference Name: IEEE Transactions on Haptics, pp. 118–133. ISSN: 2329-4051. DOI: 10.1109/TOH.2023.3253856. URL: https://ieeexplore.ieee.org/document/10064154 (visited on 04/23/2024).

[11] Gregory Tholey, Jaydev P. Desai, and Andres E. Castellanos. "Force Feedback Plays a Significant Role in Minimally Invasive Surgery". In: *Annals of Surgery* 241.1 (Jan. 2005), pp. 102–109. ISSN: 0003-4932. DOI: 10.1097/01.sla.0000149301.60553.1e. URL: https://www.ncbi.nlm.nih.gov/pmc/articles/PMC1356852/ (visited on 05/15/2024).

[12] Oleg Gerovich, Panadda Marayong, and Allison M. Okamura. "The effect of visual and haptic feedback on computer-assisted needle insertion". In: *Computer Aided Surgery* (Jan. 1, 2004). Publisher: Taylor & Francis. DOI: 10.3109/10929080500190441. URL: https://www.tandfonline.com/doi/abs/10.3109/10929080500190441 (visited on 05/07/2024).

[13] John V. Draper, David B. Kaber, and John M. Usher. "Telepresence". In: *Human Factors* 40.3 (Sept. 1, 1998). Publisher: SAGE Publications Inc, pp. 354–375. ISSN: 0018-7208. DOI: 10.1518/001872098779591386. URL: https://doi.org/10.1518/001872098779591386 (visited on 06/07/2024).

[14] D.A. Lawrence. "Stability and transparency in bilateral teleoperation". In: *IEEE Transactions on Robotics and Automation* 9.5 (Oct. 1993). Conference Name: IEEE Transactions on Robotics and Automation, pp. 624–637. ISSN: 2374-958X. DOI: 10.1109/70.258054. URL: https://ieeexplore.ieee.org/document/258054 (visited on 06/07/2024).

[15] Michel Franken et al. "Bilateral Telemanipulation With Time Delays: A Two-Layer Approach Combining Passivity and Transparency". In: *IEEE Transactions on Robotics* 27.4 (Aug. 2011), pp. 741–756. ISSN: 1552-3098, 1941-0468. DOI: 10.1109/TRO.2011.2142430. URL: http://ieeexplore.ieee.org/document/5784345/ (visited on 06/06/2024).

[16] B. Hannaford and Jee-Hwan Ryu. "Time-domain passivity control of haptic interfaces". In: *IEEE Transactions on Robotics and Automation* 18.1 (Feb. 2002). Conference Name: IEEE Transactions on Robotics and Automation, pp. 1–10. ISSN: 2374-958X. DOI: 10.1109/70.988969. URL: https://ieeexplore.ieee.org/document/988969 (visited on 06/06/2024).

[17] L.B. Rosenberg. "Virtual fixtures: Perceptual tools for telerobotic manipulation". In: *Proceedings of IEEE Virtual Reality Annual International Symposium*. Proceedings of IEEE Virtual Reality Annual International Symposium. Sept. 1993, pp. 76–82. DOI: 10.1109/VRAIS.1993.380795. URL: https://ieeexplore.ieee.org/abstract/document/380795 (visited on 06/06/2024).

[18] Jake J. Abbott, Panadda Marayong, and Allison M. Okamura. "Haptic Virtual Fixtures for Robot-Assisted Manipulation". In: *Robotics Research*. Ed. by Sebastian Thrun, Rodney Brooks, and Hugh Durrant-Whyte. Vol. 28. Series Title: Springer Tracts in Advanced Robotics. Berlin, Heidelberg: Springer Berlin Heidelberg, 2007, pp. 49–64. ISBN: 978-3-540-48110-2. DOI: 10.1007/978-3-540-48113-3_5. URL: http://link.springer.com/10.1007/978-3-540-48113-3_5 (visited on 06/06/2024).

[19] A. Bettini et al. "Vision-assisted control for manipulation using virtual fixtures". In: *IEEE Transactions on Robotics* 20.6 (Dec. 2004). Conference Name: IEEE Transactions on Robotics, pp. 953–966. ISSN: 1941-0468. DOI: 10.1109/TRO.2004.829483. URL: https://ieeexplore.ieee.org/document/1362691 (visited on 06/06/2024).

[20] Kevin Huang et al. "Evaluation of haptic guidance virtual fixtures and 3D visualization methods in telemanipulation—a user study". In: *Intelligent Service Robotics* 12.4 (Oct. 1, 2019), pp. 289–301. ISSN: 1861-2784. DOI: 10.1007/s11370-019-00283-w. URL: https://doi.org/10.1007/s11370-019-00283-w (visited on 06/07/2024).

[21] Bernhard Bischof and Andreas Kugi. "Dynamic Virtual Fixtures Based on Path Following Control". In: *IFAC-PapersOnLine*. 11th IFAC Symposium on Nonlinear Control Systems NOLCOS 2019 52.16 (Jan. 1, 2019), pp. 424–429. ISSN: 2405-8963. DOI: 10.1016/j.ifacol.2019.11.817. URL: https://www.sciencedirect.com/science/article/pii/S2405896319318245 (visited on 06/07/2024).

[22] J.J. Abbott and A.M. Okamura. "Pseudo-admittance Bilateral Telemanipulation with Guidance Virtual Fixtures". In: *2006 14th Symposium on Haptic Interfaces for Virtual Environment and Teleoperator Systems*. 2006 14th Symposium on Haptic Interfaces for Virtual Environment and Teleoperator Systems. ISSN: 2324-7355. Mar. 2006, pp. 169–175. DOI: 10.1109/HAPTIC.2006.1627057. URL: https://ieeexplore.ieee.org/document/1627057 (visited on 06/07/2024).

[23] Jake J Abbott. "Virtual Fixtures for Bilateral Telemanipulation". In: ().

[24] Ming Li, Masaru Ishii, and Russell H Taylor. "Spatial Motion Constraints Using Virtual Fixtures Generated by Anatomy". In: ().

[25] P. Schleer, S. Drobinsky, and K. Radermacher. "Evaluation of Different Modes of Haptic Guidance for Robotic Surgery". In: *IFAC-PapersOnLine*. 2nd IFAC Conference on Cyber-Physical and Human Systems CPHS 2018 51.34 (Jan. 1, 2019), pp. 97–103. ISSN: 2405-8963. DOI: 10.1016/j.ifacol.2019.01.035. URL: https://www.sciencedirect.com/science/article/pii/S2405896319300370 (visited on 06/05/2024).

[26] J. Smisek, M. M. van Paassen, and A. Schiele. "Haptic guidance in bilateral teleoperation: Effects of guidance inaccuracy". In: *2015 IEEE World Haptics Conference (WHC)*. 2015 IEEE World Haptics Conference (WHC). June 2015, pp. 500–505. DOI: 10.1109/WHC.2015.7177762. URL: https://ieeexplore.ieee.org/document/7177762 (visited on 06/05/2024).

[27] Jeroen van Oosterhout et al. "Haptic Shared Control in Tele-Manipulation: Effects of Inaccuracies in Guidance on Task Execution". In: *IEEE Transactions on Haptics* 8.2 (Apr. 2015). Conference Name: IEEE Transactions on Haptics, pp. 164–175. ISSN: 2329-4051. DOI: 10.1109/TOH.2015.2406708. URL: https://ieeexplore.ieee.org/document/7047839 (visited on 06/05/2024).

[28] Mehdi Jafari and Habib Molaei. "Spherical Linear Interpolation and Bézier Curves". In: *General Scientific Researches* 2 (Jan. 1, 2014).

[29] Barrera T, Hast Anders, and Bengtsson Ewert. “Incremental spherical linear interpolation”. In: *Linköping electronic conference proceedings*. SIGRAD 2004: Special theme - Environmental visualization. Vol. 13. ISSN: 1650-3686. 2004. URL: https://res.slu.se/id/publ/5605 (visited on 12/30/2024).

[30] Adam Wittek et al. “Mathematical modeling and computer simulation of needle insertion into soft tissue”. In: *PLoS ONE* 15.12 (Dec. 22, 2020), e0242704. ISSN: 1932-6203. DOI: 10.1371/journal.pone.0242704. URL: https://www.ncbi.nlm.nih.gov/pmc/articles/PMC7755224/ (visited on 01/21/2025).

[31] Guoyi Wu et al. “Importance of tumor size at diagnosis as a prognostic factor for hepatocellular carcinoma survival: a population-based study”. In: *Cancer Management and Research* 10 (Oct. 10, 2018), pp. 4401–4410. ISSN: 1179-1322. DOI: 10.2147/CMAR.S177663. URL: https://www.ncbi.nlm.nih.gov/pmc/articles/PMC6188157/ (visited on 12/27/2024).

[32] John Brooke. “SUS - A quick and dirty usability scale”. In: ().

[33] Ellen R. Girden. *ANOVA: Repeated measures*. ANOVA: Repeated measures. Pages: vi, 77. Thousand Oaks, CA, US: Sage Publications, Inc, 1992. vi, 77. ISBN: 0-8039-4257-5 (Paperback).

[34] Amitav Banerjee et al. “Hypothesis testing, type I and type II errors”. In: *Industrial Psychiatry Journal* 18.2 (2009), pp. 127–131. ISSN: 0972-6748. DOI: 10.4103/0972-6748.62274. URL: https://www.ncbi.nlm.nih.gov/pmc/articles/PMC2996198/ (visited on 01/21/2025).

[35] Estibaliz Gómez-de Mariscal et al. “Use of the p-values as a size-dependent function to address practical differences when analyzing large datasets”. In: *Scientific Reports* 11.1 (Oct. 22, 2021). Publisher: Nature Publishing Group, p. 20942. ISSN: 2045-2322. DOI: 10.1038/s41598-021-00199-5. URL: https://www.nature.com/articles/s41598-021-00199-5 (visited on 01/20/2025).

[36] R. Likert. “A technique for the measurement of attitudes.” In: *Archives of Psychology* 22 140 (1932), pp. 55–55.

[37] Jeff Sauro and James R. Lewis. “Chapter 8 - Standardized Usability Questionnaires”. In: *Quantifying the User Experience*. Ed. by Jeff Sauro and James R. Lewis. Boston: Morgan Kaufmann, Jan. 1, 2012, pp. 185–240. ISBN: 978-0-12-384968-7. DOI: 10.1016/B978-0-12-384968-7.00008-4. URL: https://www.sciencedirect.com/science/article/pii/B9780123849687000084 (visited on 01/19/2025).

[38] James Diebel. “Representing Attitude: Euler Angles, Unit Quaternions, and Rotation Vectors”. In: ().